引用本文:李奇,吴勇,乔磊.深部中阶煤孔结构的压汞—液氮联合表征及孔隙分形特征[J].石油实验地质,2025,47(1):130-142.DOI:10.11781/sysydz2025010130.

LI Qi,WU Yong,QIAO Lei.Combined characterization of pore structure in deep medium-rank coal using mercury intrusion and liquid nitrogen adsorption methods and its pore fractal characteristics[J].Petroleum Geology & Experiment,2025,47(1):130-142.DOI:10.11781/sysydz2025010130.

深部中阶煤孔结构的压汞—液氮联合表征及孔隙分形特征

李 奇[1,2,3],吴 勇[1],乔 磊[3]

1. 成都理工大学 环境与土木工程学院,成都 610059;
2. 温州理工学院 ,浙江 温州 325006;
3. 浙江省岩石力学与地质灾害重点实验室,浙江 绍兴 312000

摘要:为研究深部中阶煤的孔隙结构特征与孔隙分形规律,利用压汞法和液氮吸附法对沈阳红阳三矿、开滦林西矿、淮南新集二矿和平顶山平煤六矿等典型深部开采矿区的主采煤层煤样进行了孔径、孔容、比表面积等参数测试,基于 Menger 海绵模型和 FHH 模型进行了孔隙分形规律的研究。结果表明:①基于压汞法的孔隙结构参数测试中平均孔径 31.10~34.70 nm,总孔容 0.048 3 ~0.059 4 mL/g,总比表面积 5.590 9 ~7.652 8 m^2/g,得出典型深部开采矿区的主采煤层孔隙发育比较接近;孔容分布以大孔孔容占主导,微孔与过渡孔孔容比重相当,中孔的孔容分布相对较小,表明大孔孔隙连通性较好,中孔较为闭塞;比表面积分布以微孔为主,占比达 70%以上,而中孔和大孔的比重甚微,可见微孔吸附能力最强,不利于深部煤层瓦斯治理;Menger 海绵模型分形维数介于 2.6~3 之间,表明孔隙形状很不规则,孔隙较为复杂,整体上孔隙表面较为粗糙。②基于液氮吸附法测试的有效孔径范围为 3~177 nm,总孔容与比表面积不同的矿区差异明显,孔容分布以过渡孔和中孔为主,微孔分布较低,大孔为 0,表明利用液氮吸附法对于中孔、过渡孔有很好的表征,而难以表征大孔结构,且微孔的孔隙连通性较差;比表面积分布中主要为过渡孔、微孔和中孔,大孔为 0,其中以过渡孔为主,且其吸附能力也较强;FHH 模型分形维数介于 2.0~2.7,结构较为简单规则。③讨论了深部中阶煤孔隙结构差异性,其中压汞法和液氮法的孔隙结构参数(比表面积、孔容)随埋深的增加均呈非线性的凹曲线变化;Menger 海绵模型与 FHH 模型分形维数则随埋深的增加呈凸曲线的变化趋势。

关键词:深部中阶煤;压汞法;液氮吸附法;孔径结构;孔隙分形

中图分类号:TE132.2 **文献标识码**:A DOI:10.11781/sysydz2025010130

Combined characterization of pore structure in deep medium-rank coal using mercury intrusion and liquid nitrogen adsorption methods and its pore fractal characteristics

LI Qi[1,2,3], WU Yong[1], QIAO Lei[3]

1. *College of Environment and Civil Engineering, Chengdu University of Technology, Chengdu, Sichuan* 610059, *China*;
2. *Wenzhou University of Technology, Wenzhou, Zhejiang* 325006, *China*;
3. *Key Laboratory of Rock Mechanics and Geohazards of Zhejiang Province, Shaoxing, Zhejiang* 312000, *China*

Abstract: To study the pore structure and fractal characteristics of deep medium-rank coal, combined characterization using mercury intrusion and liquid nitrogen adsorption methods was conducted on coal samples from the main coal seams in typical deep mining areas, including Shenyang Hongyang Third Mine, Kailuan Linxi Mine, Huainan Xinji Second Mine, and Pingdingshan Pingmei Sixth Mine. Parameters such as pore size, pore volume, and specific surface area were obtained, and the pore fractal characteristics were studied based on the Menger sponge model and the FHH model. The results showed that: (1) Among the pore structure parameters tested with mercury intrusion

收稿日期(Received):2024-01-05;**修订日期(Revised)**:2024-11-29;**出版日期(Published)**:2025-01-28。

作者简介:李奇(1985—),男,博士,副教授,主要从事矿山安全与地质工程等相关方向的研究。E-mail:907108513@qq.com。

通信作者:乔磊(1994—),男,硕士,助理实验师,主要从事岩石力学特性及试验仪器开发方面的研究。E-mail:qiaolei@usx.edu.cn。

基金项目:浙江省岩石力学与地质灾害重点实验室开放基金项目(ZJRMG-2023-01)资助。

© Editorial Office of Petroleum Geology & Experiment. This is an open access article under the CC BY-NC-ND license.

method, the average pore size ranged from 31.10 to 34.70 nm, pore volume from 0.048 3 to 0.059 4 mL/g, and specific surface area from 5.590 9 to 7.652 8 m^2/g. The pore development in the main coal seams of typical deep mining areas was relatively similar. The pore volume distribution was dominated by macropores, with micropores and transition pores contributing roughly equally, and mesopores having a relatively small distribution. This indicated that macropores had better connectivity and mesopores were more closed. Micropores accounted for more than 70% of the total specific surface area, while the proportions of mesopores and macropores were minimal, indicating that micropores had the strongest adsorption capacity, which was negatively affected gas management in deep coal seams. The fractal dimensions based on the Menger sponge model ranged from 2.6 to 3.0, indicating irregular pore shapes, complex pore structures, and generally rough pore surfaces. (2) The effective pore size tested using liquid nitrogen adsorption method ranged from 3 to 177 nm with significant differences in total pore volume and specific surface area among the mining areas. Pore volume distribution was dominated by transition pores and mesopores, with a lower distribution of micropores and no macropores. This indicated that liquid nitrogen adsorption was effective for characterizing mesopores and transition pores but struggled to characterize macropore structures. Moreover, the connectivity of micropores was relatively poor. The specific surface area was mainly composed of transition pores, micropores, and mesopores, with no macropores. Among them, transition pores were mostly dominant and had relatively strong adsorption capacity. The fractal dimensions based on the FHH model ranged from 2.0 to 2.7, indicating a relatively simple and regular structure. (3) The differences in pore structures of deep medium-rank coal were discussed. The pore structure parameters (specific surface area and pore volume) determined by mercury intrusion and liquid nitrogen adsorption methods showed a non-linear concave curve variation with increasing burial depth. The fractal dimensions derived from the Menger sponge model and the FHH model showed a convex curve trend with increasing burial depth.

Key words: deep medium-rank coal; mercury intrusion method; liquid nitrogen adsorption method; pore size structure; pore fractal characteristics

煤是一种非均质性很强的多孔介质[1-4],其表面是瓦斯吸附、解吸过程的主要场所,研究煤体的孔径尺寸、孔径结构和孔隙分形对于煤层气预测、评价与开发,煤矿瓦斯灾害治理具有重要意义。目前,对煤的孔径结构采用的研究方法主要为有损测试法和无损测试法两大类。有损测试法是将流体介质高压注入或低温吸附到煤体孔隙中,通过计算流体介质的体积确定煤的孔隙体积,如广泛应用的压汞法[5-6]、液氮吸附法[7-8]和低温二氧化碳吸附法[9]等,但高压或低温流体介质进入样品后,也破坏了部分原生孔隙;无损测试法是利用显微镜观测、射线探测等技术,不介入煤体内部实现孔隙的研究,如光学显微镜[10]、原子力显微镜[11]、场发射电子显微镜[12-13]、环境扫描电子显微镜等显微观测[14]、X 射线计算机断层扫描[15]、核磁共振[16-17]和小角度 X 射线散射[18-19]等,其存在精度低、误差大、适应性差等局限,需联合传统方法表征。传统欧氏几何可描述表面光滑、均质的对象,但难以准确表征粗糙的形状[20],直到 1975 年 MANDELBROT 创立了分形几何理论[21-22],实现了对粗糙形状对象的准确表征,为描述煤体孔隙结构的复杂性提供了重要方法。

近年来多种分形模型大量应用于煤体孔隙结构研究,如陈向军等[23]利用海绵模型分析了不同变质程度煤孔隙结构,发现煤孔隙在不同孔径段具有不同的分形特征;王秀娟等[24]采用热力学分形模型,计算了煤的渗流孔的分形维数,并探讨了分形维数与渗透率的关系;杨师宇等[25]运用谢尔宾斯基模型定量探讨了煤储层渗流孔孔隙结构特征及其影响因素,并进行了煤岩渗透率预测;刘怀谦等[26]运用毛细管模型[27-29]分析了海湾煤矿 5-2 煤和顾北煤矿中央 1 煤孔隙结构复杂程度,同时分析了现有模型的适用性并提出了新方法;薛海腾等[30]利用 FHH 模型[31]研究了黔西突出煤的微观孔隙分形特征与其吸附性能及渗透率的关系;周三栋等[32]通过 BET 模型分形[33-34]分析了低阶煤的吸附孔特征,确定了适合低阶煤吸附孔的孔隙分形模型及分形维数与孔结构、吸附性能的关联性;熊益华等[35]深入研究煤和页岩的微孔特征,基于孔径分布密度函数模型[36],对比分析了煤和页岩微孔结构的分形特征,尽管发现煤的微孔比表面积均远大于页岩,但其孔径分布、孔隙结构比页岩简单,微孔分形维数小于页岩。上述学者的研究成果更多关注于当前开采的浅部煤层,深部煤体尤其是对

千米级埋深煤层的孔隙结构研究鲜有关注,相关成果甚少,同时单一的分形模型也难以全面有效地评价煤体孔隙的复杂性。为此,本文以千米级赋存煤层为研究对象,利用压汞法—液氮法联合表征,深入分析深部中阶煤层的孔径结构特征以及孔隙分形规律,冀望为深部开采工程提供有效的理论依据。

1 试样来源与基础参数测试

测试煤样取自沈阳红阳三矿、开滦林西矿、淮南新集二矿和平顶山平煤六矿等典型深部开采矿区主采煤层,煤样工业分析指标依据国家标准《煤的工业分析方法:GB/T 212—2008》进行测试,按《中国煤炭分类:GB/T 5751—2009》对煤种进行分类,测试结果如表 1。

2 深部中阶煤的孔径结构联合表征

2.1 基于压汞法的孔结构特征

高压压汞法利用美国麦克仪器公司生产的 AUTOPORE IV 9505 型全自动压汞仪进行测试,高压分析可达 227.53 MPa,孔径分布范围可达 5 nm~950 μm。实验前将煤样筛分 10~20 目各 5 g,在 100 ℃下真空干燥 24 h,再抽真空 12 h。

对煤体而言汞为非润湿液体,煤体孔隙中受到外力后会平衡毛细管力影响,从而进入煤体。毛细管力大小与孔隙尺寸相关,增加汞注入压力使其不断进入煤体孔隙,通过测试注汞体积,反算孔径结构[37-41]。在理想的圆形断面孔隙中,孔隙半径与汞压力满足 Washburn 方程:

$$r=(-2\sigma\cos\theta)/P \quad (1)$$

式中:r 为煤中孔隙半径,单位 m;σ 为汞的界面张力,取 0.48 J/m^2;θ 为汞对煤的润湿边缘角,取 140°;P 为绝对进汞压力,单位 MPa。

按照上述方法对煤样进行压汞测试,压汞试验结果如表 2,压汞曲线如图 1 所示。

据表 2,各矿区煤样孔径大小相近,平均孔径范围为 31.10~34.70 nm,总孔容(V_T)为 0.048 3~0.059 4 mL/g,总比表面积(S_T)为 5.590 9~7.652 8 m^2/g,结果表明 4 组煤样孔隙发育程度较为相近。

为便于开展孔径分布定量分析,本次采用霍多特十进制孔径分类标准[42]研究孔径分布规律(即孔径小于 10 nm 为微孔,10~100 nm 为过渡孔,100~1 000 nm 为中孔,大于 1 000 nm 为大孔),计算出高压压汞试验孔容分布(表 3)和比表面积分布(表 4)。

根据表 3,大孔孔容占比最大(57.44%~62.47%),微孔(15.52%~17.51%)、过渡孔(16.15%~17.31%)孔容相对较小,中孔的孔容最小(4.57%~9.93%)。结合孔容—孔径分布曲线(图 1)看出累计孔容曲线中部平缓,两端陡峭,阶段孔容曲线形态呈中部低两端高的不对称 U 型且右端出现最大值,表明典型深部矿区煤样的大孔分布占主导,微孔、过渡孔孔容居中,中孔的分布比较少。

根据表 4,煤样的比表面积主要来自于微孔和过渡孔,其中微孔占主导(72.96%~74.27%),中孔和大孔的比重甚微,从比表面积—孔径分布曲线(图 2)看出,随着孔径的增加比表面积逐渐减小,表明典型深部矿区煤层的微孔吸附能力最强。

2.2 基于海绵模型的孔径分形特征

大孔孔径分形特征基于 Menger 海绵模型[23]分析,其原理为假设将边长为 R 的立方体设为初始元,将该立方体均分成m^3个小立方体,则每个小

表 1 典型矿区深部主采煤层基础参数

Table 1 Basic parameters of deep main coal seams in typical mining areas

试样编号	试样来源	采样煤层	埋深/m	工业分析指标/%				煤种
				M_{ad}	A_{ad}	V_{ad}	FC_{ad}	
1#	红阳三矿	7#煤	1 100	0.73	11.40	11.93	75.94	瘦煤
2#	林西矿	12 煤	950	0.90	11.17	18.85	69.08	焦煤
3#	新集二矿	9 煤	800	2.22	26.04	28.81	42.93	气煤
4#	平煤六矿	戊 8 煤	940	1.70	13.74	29.27	55.29	1/3 焦煤

注:M_{ad}.空气干燥基水分;A_{ad}.空气干燥基灰分;V_{ad}.空气干燥基挥发分;FC_{ad}.空气干燥基固定碳。

表 2 典型矿区深部主采煤层孔径参数(压汞法)

Table 2 Pore size parameters of deep main coal seams in typical mining areas (mercury intrusion method)

试样编号	样品质量/g	孔隙度/%	V_T/(mL/g)	S_T/(m^2/g)	体积中值孔径/nm	面积中值孔径/nm	平均孔径/nm
1#	1.196 3	7.720 4	0.059 4	7.652 8	44 676.40	7.700	31.10
2#	1.162 6	6.360 6	0.048 3	5.590 9	16 958.10	8.000	34.60
3#	1.148 8	6.588 8	0.048 8	5.980 5	13 595.50	7.600	32.60
4#	1.140 0	7.014 1	0.053 1	6.126 3	32 597.70	8.000	34.70

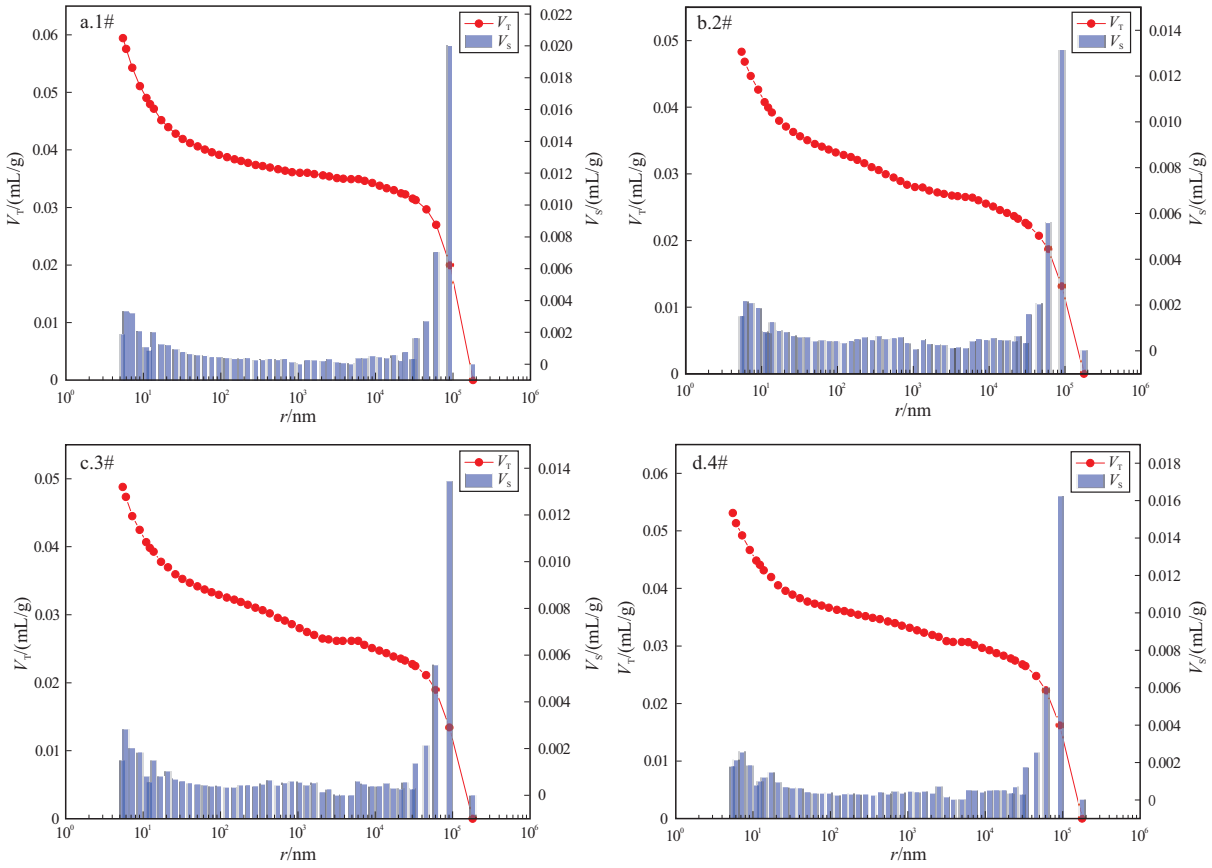

图 1　典型矿区深部主采煤层孔容分布(压汞法)

Fig.1　Pore volume distribution in deep main coal seams of typical mining areas (mercury intrusion method)

表 3　典型矿区深部主采煤层孔容分布计算表(压汞法)

Table 3　Calculation of pore volume distribution in deep main coal seams of typical mining areas (mercury intrusion method)

试样编号	总孔容(V_T)/(mL/g)	分阶段孔容(V_S)/(mL/g)				分阶段孔容占比/%			
		V_1	V_2	V_3	V_4	V_1/V_T	V_2/V_T	V_3/V_T	V_4/V_T
1#	0.059 4	0.010 4	0.010 3	0.002 7	0.036 0	17.51	17.31	4.57	60.61
2#	0.048 3	0.007 5	0.007 9	0.004 8	0.028 0	15.61	16.45	9.93	58.00
3#	0.048 8	0.008 1	0.008 1	0.004 5	0.028 1	16.67	16.66	9.23	57.44
4#	0.053 1	0.008 2	0.008 6	0.003 1	0.033 2	15.52	16.15	5.86	62.47

注:表中 V_1、V_2、V_3、V_4分别指微孔(r<10 nm)、过渡孔(10≤r<100 nm)、中孔(100≤r<1 000 nm)、大孔(>1 000 nm)的孔容。

表 4　典型矿区深部主采煤层比表面积分布计算表(压汞法)

Table 4　Calculation of specific surface area distribution in deep main coal seams of typical mining areas (mercury intrusion method)

试样编号	总比表面积(S_T)/(m^2/g)	分阶段比表面积(S_S)/(m^2/g)				分阶段比表面积占比/%			
		S_1	S_2	S_3	S_4	S_1/S_T	S_2/S_T	S_3/S_T	S_4/S_T
1#	7.652 8	5.671 1	1.936 3	0.041 0	0.004 4	74.10	25.30	0.54	0.06
2#	5.590 9	4.079 1	1.444 4	0.062 0	0.005 4	72.96	25.83	1.11	0.10
3#	5.980 5	4.441 7	1.476 8	0.055 0	0.007 0	74.27	24.69	0.92	0.12
4#	6.126 3	4.471 9	1.607 4	0.039 2	0.007 8	73.00	26.24	0.64	0.12

注:表中 S_1、S_2、S_3、S_4分别指微孔、过渡孔、中孔和大孔的比表面积。

立方体的边长 $r_1=R/m$,如任意剔除 n 个小立方体,余下立方体数量则为 $N_{b1}=m^3-n$。不断迭代重复上述做法,再将余下边长为 R/m 的立方体再次均分为 m^3个微小立方体,则每个立方体的边长$r_2=R/m^2$,

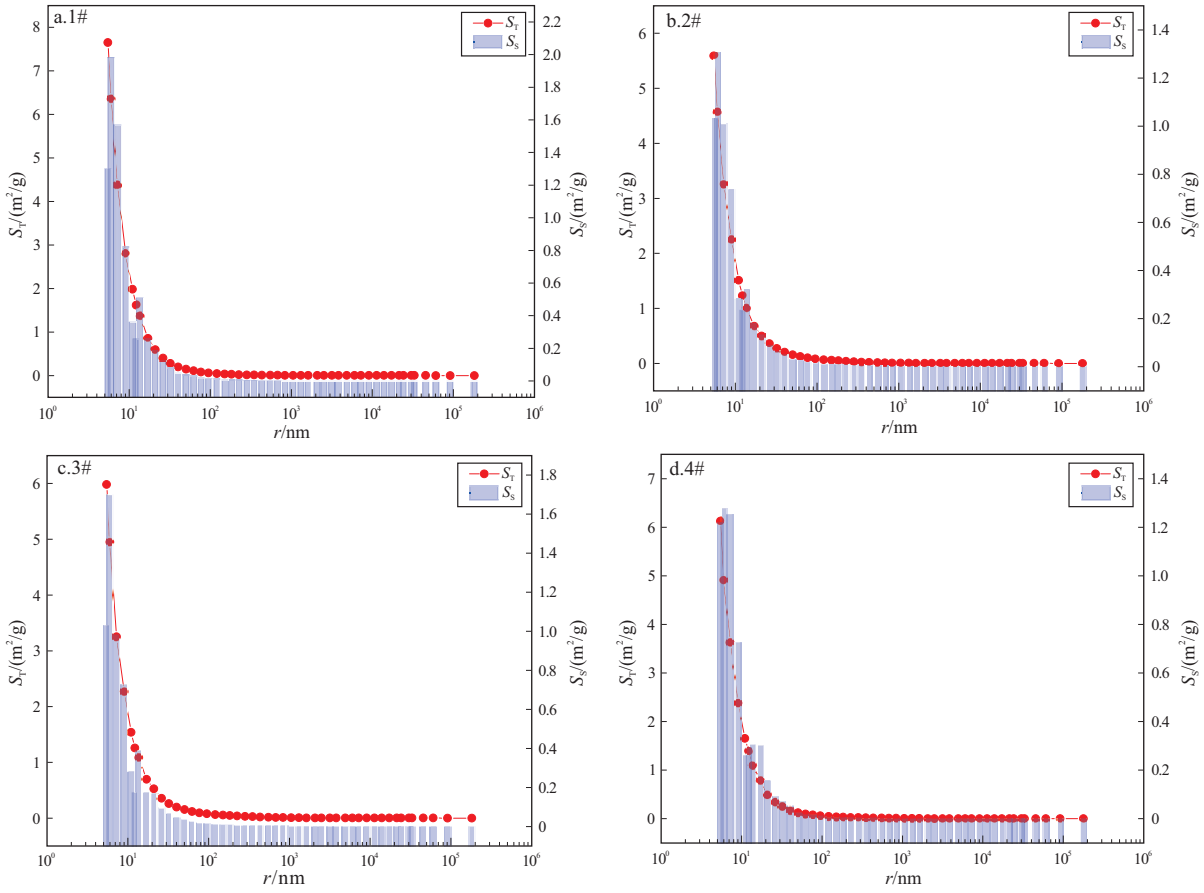

图 2 典型矿区深部主采煤层比表面积分布(压汞法)

Fig.2 Specific surface area distribution in deep main coal seams of typical mining areas (mercury intrusion method)

再任意剔除其中的 n 个小立方体,此时剩余的立方体数量为 $N_{b2}=(m^3-n)^2$。同理,经过 k 次迭代后,最终剩余小立方体的数量为 $N_{bk}=(m^3-n)^k$,边长为 $r_k=R/m^k$。那么微立方体数量可计为:

$$N_{bk}=\left(\frac{r_k}{R}\right)^{-D} \tag{2}$$

式中:N_{bk}为 k 次迭代后剩余小立方体的数量,单位个;D 为孔隙介质分形维数,无量纲;r_k为 k 次迭代后立方体边长,单位 m;R 为初始元立方体边长,单位 m。

立方体的总体积为:

$$V_k=r_k^{\ 3}N_{bk}=\frac{r_k^{3-D}}{R^{-D}} \tag{3}$$

式中:V_k为立方体的总体积,单位 m^3;r_k为 k 次迭代后立方体边长,单位 m;N_{bk}为 k 次迭代后剩余小立方体的数量,单位个;R 为初始元立方体边长,单位 m;D 为孔隙介质分形维数,无量纲。

且有当 $k\to\infty$时,$V_k\to V_r$,V_r为多孔介质的骨架体积。

则对上式求导得到:

$$\mathrm{d}V/\mathrm{d}r\propto r^{2-D} \tag{4}$$

式中:V 为煤的孔隙体积,单位 m^3;r 为煤中孔隙半径,单位 m;D 为孔隙介质分形维数,无量纲。

根据 Washburn 方程得到:

$$P=0.735\ 4/r \tag{5}$$

求导得:$P\mathrm{d}r+r\mathrm{d}P=0$,代入(3)式得到:

$$\mathrm{d}V/\mathrm{d}P\propto r^2\cdot r^{2-D}\propto r^{4-D} \tag{6}$$

两侧取对数得:

$$\lg(\mathrm{d}V/\mathrm{d}P)\propto(4-D)\lg r\propto(D-4)\lg P \tag{7}$$

由此,可通过 $\lg(\mathrm{d}V/\mathrm{d}P)$ 与 $\lg P$ 绘制散点图,利用斜率求算分形维数。

据图 3、表 5 可知,几组试样分形维数介于 2.6~3 之间,表明孔隙形状很不规则,孔隙较为复杂,1#最小,3#与 4#次之,2#最大,孔隙表面也最为粗糙。

2.3 基于液氮吸附法的孔结构特征

液氮吸附法试验过程参照国家标准《压汞法和气体吸附法测定固体材料孔径分布和孔隙度第 1 部分:压汞法GB/T21650.2—2008》,利用

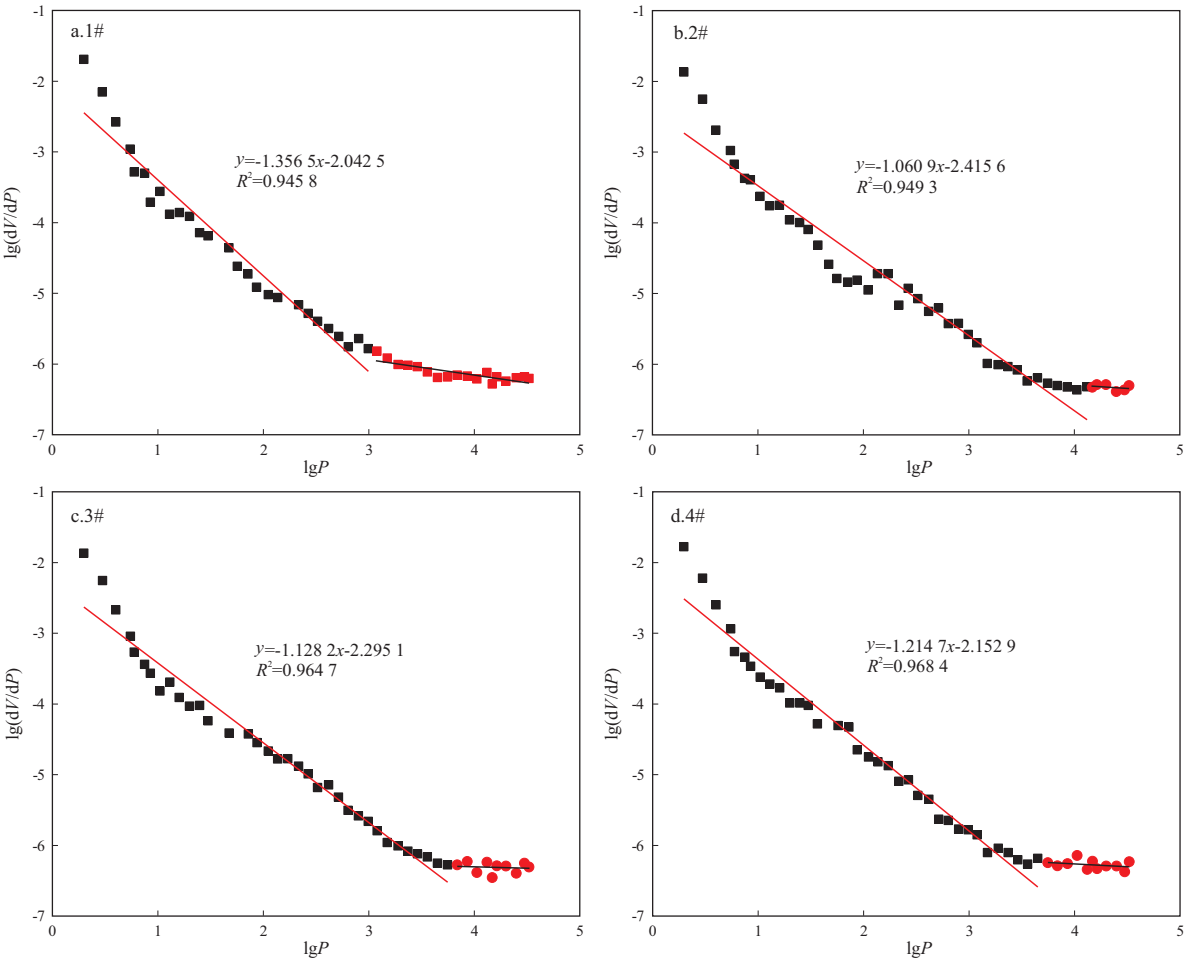

图 3　典型矿区深部主采煤层海绵模型

Fig.3　Sponge models of deep main coal seams in typical mining areas

表 5　典型矿区深部主采煤层海绵模型分形维数计算表

Table 5　Calculation of fractal dimensions of Sponge model for deep main coal seams in typical mining areas

试样编号	拟合方程	拟合度(R^2)	方程斜率(K)	分形维数(D_S)
1#	$y=-1.356\ 5x-2.042\ 5$	0.945 8	−1.356 5	2.643 5
2#	$y=-1.060\ 9x-2.415\ 6$	0.949 3	−1.060 9	2.939 1
3#	$y=-1.128\ 2x-2.295\ 1$	0.964 7	−1.128 2	2.871 8
4#	$y=-1.214\ 7x-2.152\ 9$	0.968 4	−1.214 7	2.735 3

ASAP2020 型全自动比表面与孔径分析仪进行测试,筛分 40~60 目煤样各 5 g,在 100 ℃下真空干燥 24 h,抽真空 12 h,实验温度为−196.15 ℃,相对压力为 0.01~0.999。

从液氮吸附—脱附曲线(图 4)分析,各煤样曲线均出现了不同形态的滞后环,参照国际理论和应用化学联合会分类标准[43],1#、2#、4#属于狭缝孔,3#属于堆积狭缝孔。图中 1#样吸附能力最低,最大吸附量为 1.134 8 mL/g;2#、4#次之,分别为2.560 6、2.043 2 mL/g;3#吸附能力最强、最大,吸附量为 5.733 2 mL/g。液氮法孔径测试结果见表 6 与表 7,孔径与孔容、比表面积分布见图 5、图 6。

据表 6 和图 5,过渡孔与中孔的孔容占主导,有效孔径范围内阶段孔容随着孔径的增大而增大,1#试样测定的有效孔径范围介于 8~177 nm 之间,在 177 nm 附近阶段孔容最大,为 1.043 6 mL/mg,累计孔容为 1.801 3 mL/mg;2#试样有效孔径范围介于 4~150 nm 之间,在 150 nm 附近阶段孔容最大,达 2.060 2 mL/mg,累计孔容为 3.838 8 mL/mg;3#试样有效孔径范围介于 3~150 nm 之间,在 150 nm附近阶段孔容最大,达3.314 0 mL/mg,累计孔容为 8.199 1 mL/mg;4#试样有效孔径范围介于 5~153 nm 之间,在 153 nm 附近阶段孔容最大,达 1.697 4 mL/mg,累计孔容为 3.117 0 mL/mg,表明

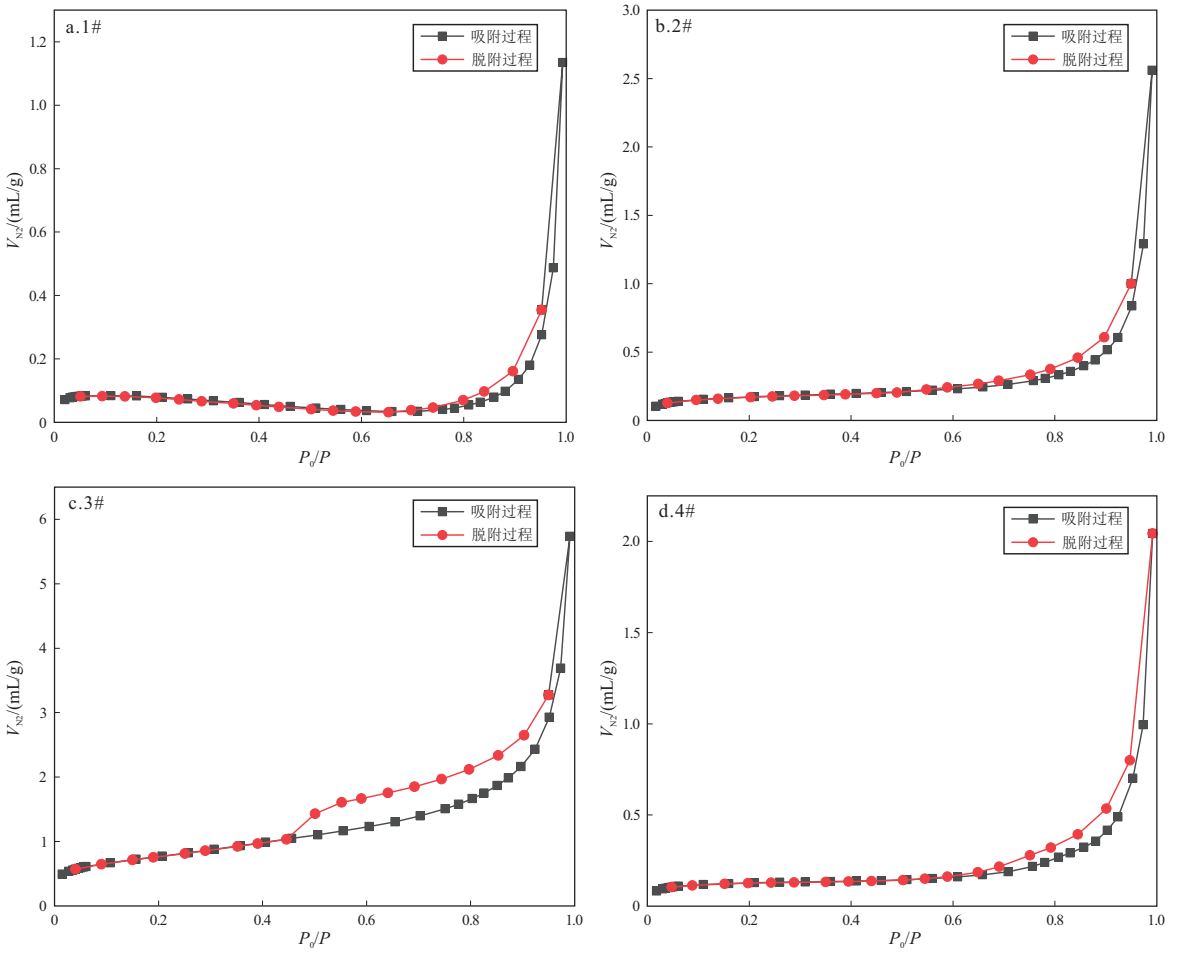

图 4 典型矿区深部主采煤层液氮吸附—脱附曲线

Fig.4 Liquid nitrogen adsorption and desorption curves of deep main coal seams in typical mining areas

表 6 典型矿区深部主采煤层孔容分布计算表(液氮法)

Table 6 Calculation of pore volume distribution in deep main coal seams of typical mining areas (liquid nitrogen method)

试样编号	样品质量/g	总孔容(V_T)/(mL/mg)	分阶段孔容(V_S)/(mL/mg)				分阶段孔容占比/%			
			V_1	V_2	V_3	V_4	V_1/V_T	V_2/V_T	V_3/V_T	V_4/V_T
1#	2.794 1	1.801 3	0.003 6	0.754 1	1.043 6	0	0.20	41.86	57.94	0
2#	3.310 5	3.838 8	0.088 7	1.689 9	2.060 2	0	2.31	44.02	53.67	0
3#	2.679 4	8.199 1	1.131 2	3.753 9	3.314 0	0	13.80	45.78	40.42	0
4#	3.338 1	3.117 0	0.110 8	1.308 8	1.697 4	0	3.55	41.99	54.46	0

表 7 典型矿区深部主采煤层比表面积分布计算表(液氮法)

Table 7 Calculation of specific surface area distribution in deep main coal seams of typical mining areas (liquid nitrogen adsorption method)

试样编号	样品质量/g	总比表面积(S_T)/(m^2/g)	分阶段比表面积(S_S)/(m^2/g)				分阶段比表面积占比/%			
			S_1	S_2	S_3	S_4	S_1/S_T	S_2/S_T	S_3/S_T	S_4/S_T
1#	2.794 1	0.117 7	0.001 5	0.092 6	0.023 6	0	1.27	78.67	20.05	0
2#	3.310 5	0.324 5	0.048 1	0.221 5	0.054 9	0	14.82	68.26	16.92	0
3#	2.679 4	1.561 4	0.882 2	0.590 5	0.088 8	0	56.49	37.82	5.69	0
4#	3.338 1	0.283 5	0.056 5	0.182 9	0.044 2	0	19.93	64.51	15.56	0

液氮法测试的各试样过渡孔与中孔的连通性最好。

据图 6 与表 7,1#试样阶段比表面积主要分布于过渡孔,在 60 nm 附近阶段比表面积最大为 0.023 8 m^2/g,累计比表面积为 0.117 7 m^2/g,曲线

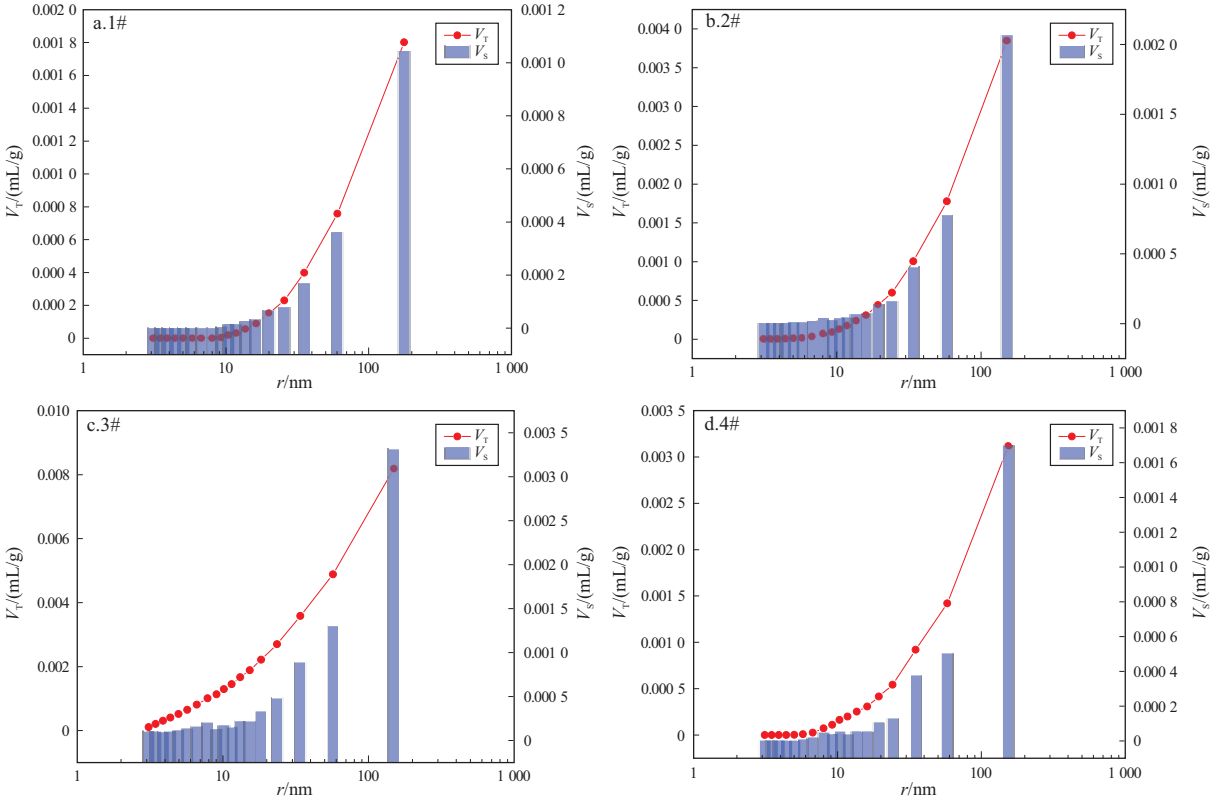

图 5　典型矿区深部主采煤层孔容分布(液氮法)

Fig.5　Pore volume distribution in deep main coal seams of typical mining areas (liquid nitrogen adsorption method)

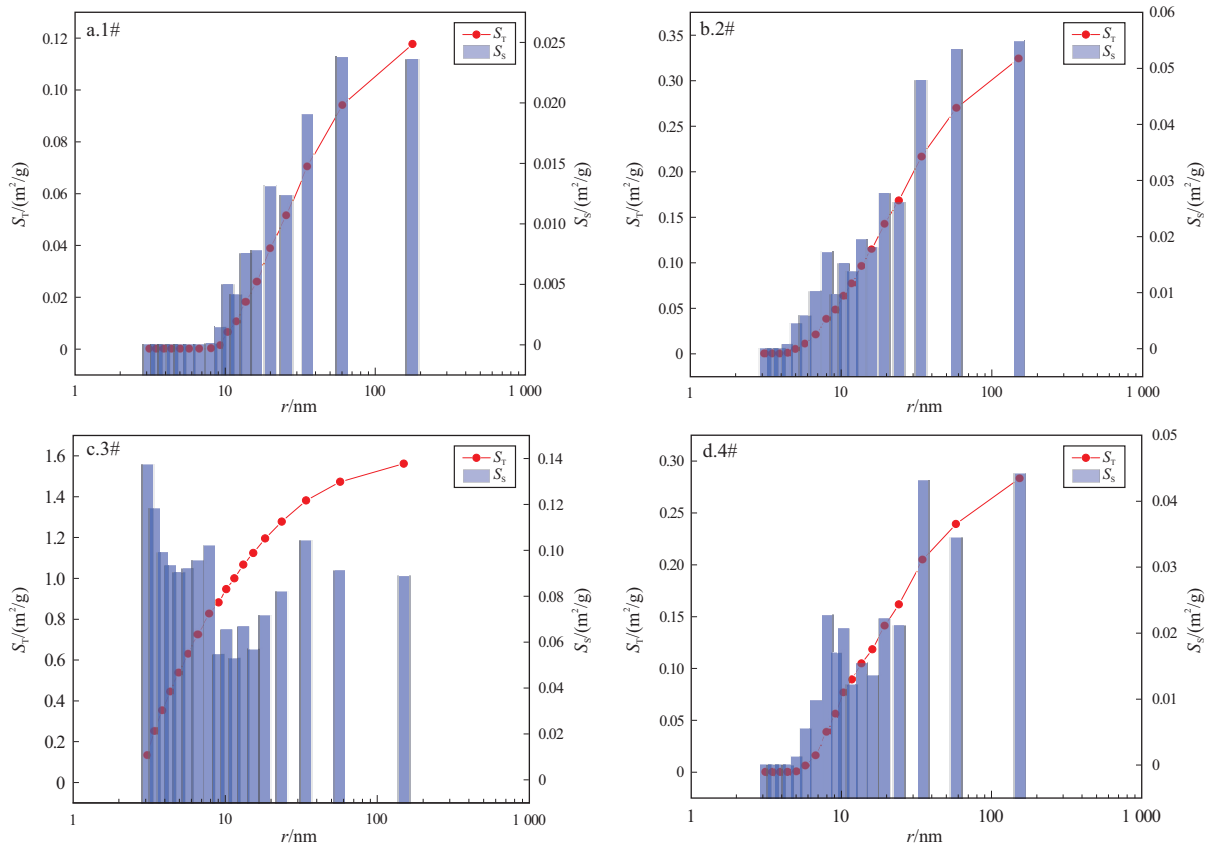

图 6　典型矿区深部主采煤层比表面积分布(液氮法)

Fig.6　Specific surface area distribution in deep main coal seams of typical mining areas (liquid nitrogen adsorption method)

呈平稳→激增→缓增的趋势变化;2#试样阶段比表面积主要分布于过渡孔,在 150 nm 附近阶段比表面积最大为0.054 9 m^2/g,累计比表面积为 0.324 5 m^2/g,曲线呈平稳→激增→缓增的趋势变化;3#试样阶段比表面积主要分布于微孔,在 3 nm 附近阶段比表面积最大,为 0.137 m^2/g,累计比表面积为 1.561 4 m^2/g,曲线呈激增→缓增的趋势变化;4#试样阶段比表面积主要分布于过渡孔,在 153 nm 附近阶段比表面积最大,为 0.044 2 m^2/g,累计比表面积为 0.283 5 m^2/g,曲线呈平稳→激增→缓增的趋势变化。

2.4 基于 FHH 模型孔径分形特征

PFEIFER 等[44]首先提出了 FHH(Frenkel Halsey Hill)模型,AVNIR 等[45]基于吸附势理论构建了气体分子在粗糙复杂的多孔介质表面的吸附模型[46],后被广泛用于多孔介质的分形维数计算。

$$\ln V = K\ln[\ln(P_0/P)] + C \tag{8}$$

$$D = K + 3 \tag{9}$$

$$D = 3(K+1) \tag{10}$$

式中:V 为液氮吸附量,单位 mL/g;K 为曲线 $\ln V - \ln[\ln(P_0/P)]$ 的斜率,无量纲;P_0 为气体吸附的饱和蒸汽压力,单位 MPa;P 为液氮吸附平衡压力,单位 MPa;C 为常数,无量纲;D 为分形维数,无量纲,取 2~3,数值越大,多孔介质表面越粗糙,反之则越光滑。

分形曲线以 $P_0/P=0.5$ 为界,当 $P_0/P<0.5$ 时,范德华力对吸附起主导作用,分形维数按 $D=3(K+1)$ 求算;当 $P_0/P>0.5$ 时,毛细凝结起主导作用,分形维数按 $D=K+3$ 求算。相对于气体与液体间的表面张力,气体与固体介质间的范德华力小到可忽略不计,因此氮气吸附于煤体时主要受控于毛细管凝聚效应,谢和平[47]认为孔表面及孔结构的分形维数一般介于 2~3,同时经计算上述 4 组数据均满足 $P_0/P>1.0$,故本次液氮吸附的孔隙分形维数按 $D=K+3$ 计算。

从图 7 和表 8 可知,几组试样中孔的分形维数介于 2.0~2.7,其中 3#样品最大,表明孔隙较为复杂,表面形状比较粗糙,非均质性较强,其他几组相对光滑,结构较为简单。

3 讨论与分析

近年来有些学者开展了煤层埋深对煤体孔隙结构影响的相关研究,陈静等[48]研究了中阶煤不同埋深的孔隙结构,得出随着埋深的增加,煤样比表面积增加,总孔容减小;冯翠荣等[49]在研究低阶煤时发现,随着埋深的增加,煤储层孔容和比表面积呈增大趋势;陆小霞等[50]得出煤层的孔容积随埋深呈现减小→增大→减小的变化趋势;刘长江等[51]发现煤样孔容和比表面积随模拟埋深增加均呈现出先增大后减小的现象。从上述研究看出,学者们对埋深致孔隙结构参数的影响还存在争议,为此需要进一步探讨深部中阶煤孔隙结构如何受埋深的影响。

3.1 埋藏深度对孔容、比表面积的影响

各试样埋深与压汞法总孔容、比表面积散点关系及拟合结果如图 8 所示,可以看出压汞法总孔容拟合曲线在 830 m 处达最小值,左侧区域分布狭小呈单调递减趋势变化,右侧分布较为广泛,总孔容随着埋深的增加而增大;总比表面积拟合曲线在 885 m 处达最小值,左侧区域呈单调递减趋势变化,同样右侧分布较为广泛呈单调递增趋势变化。

液氮法的总孔容、比表面积与埋深关系如图 9 所示,总孔容拟合曲线随着埋深的增加而增大;总比表面积拟合曲线在 1 045 m 处达最小值,左侧区域分布广泛呈单调递减趋势变化,右侧区域则呈单调递增趋势。

尽管采用不同的表征方法,埋深与孔容、埋深与比表面积的关系均呈开口朝上的凹曲线趋势变化,达到某一深度后曲线出现拐点。申建[52]认为这与地应力指标有关,拐点深度浅部主应力差较强,而深部主应力差较弱,因而出现受拐点深部影响下的孔隙结构变化的差异性。孟召平等[53]认为这与侧压系数有关,不同深度的煤层按地应力状态分伸张带、过渡带和压缩带,拐点深度附近处于过渡带,在伸张带和压缩带,孔隙结构变化截然不同。

3.2 埋藏深度对分形维数的影响

埋深与 Menger 分形维数、FHH 分形维数的关系如图 10 所示,可以看出 Menger 分形维数与埋深曲线呈凸函数变化,在 845 m 处达最大值,左侧区域呈单调增函数,右侧分布广泛呈单调递减趋势变化;而 FHH 分形维数与埋深曲线呈单调递减的趋势变化。结果表明,在 845 m 以深,分形维数均随埋深的增加而减小,深部区域煤层的孔隙结构较为简单光滑。

4 结论

(1)利用压汞法测得深部中阶煤样平均孔径 31.10~34.70 nm,总孔容 0.048 3 ~0.059 4 mL/g,总比表面积 5.590 9 ~7.652 8 m^2/g,4 组煤样孔隙

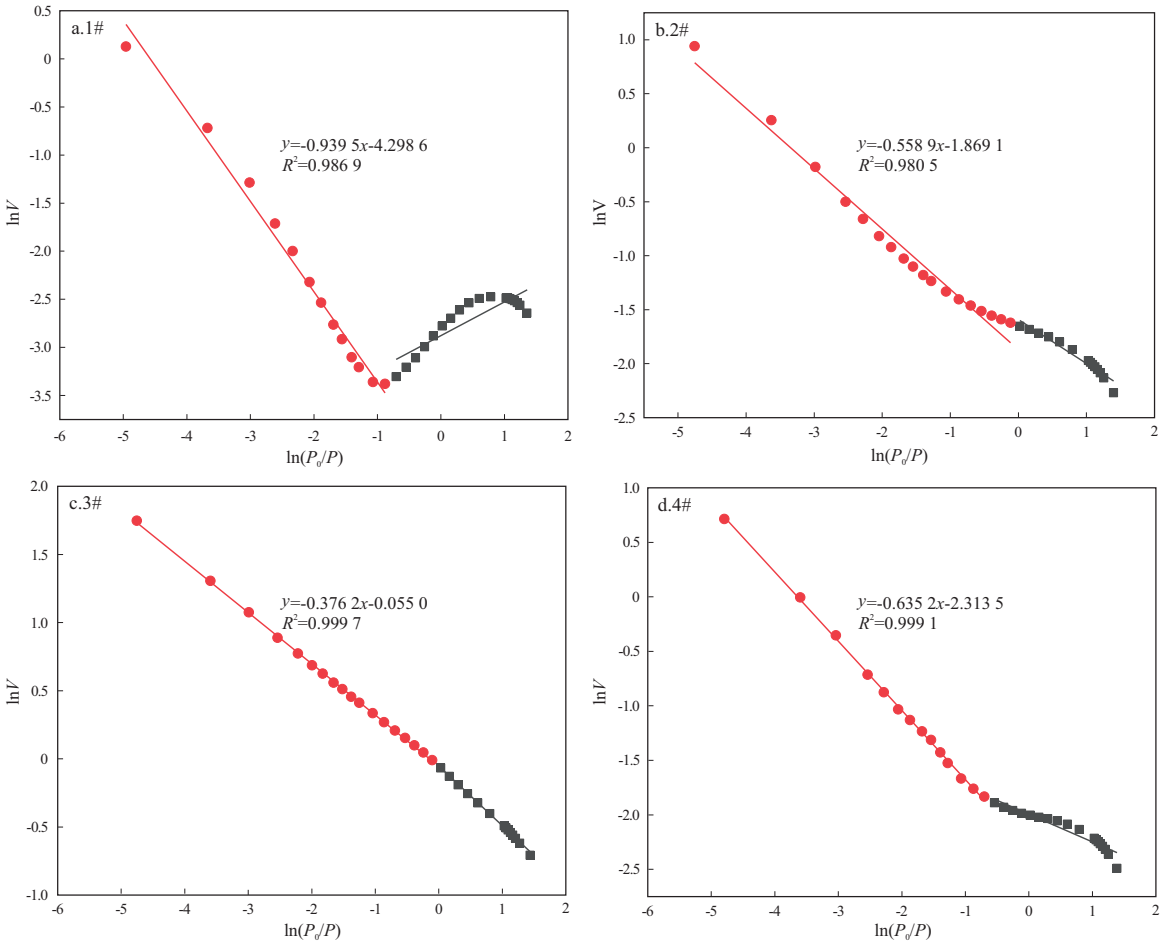

图 7　典型矿区深部主采煤层 FHH 模型分形计算

Fig.7　Fractal calculation of FHH model for deep main coal seams in typical mining areas

表 8　典型矿区深部主采煤层 FHH 模型分形维数计算表

Table 8　Calculation of fractal dimensions of FHH model for deep main coal seams in typical mining areas

试样编号	拟合方程	拟合度(R^2)	方程斜率(K)	分形维数(D_F)
1#	$y=-0.939\ 5x-4.298\ 6$	0.986 9	−0.939 5	2.060 5
2#	$y=-0.558\ 9x-1.869\ 1$	0.980 5	−0.558 9	2.441 1
3#	$y=-0.376\ 2x-0.055\ 0$	0.999 7	−0.376 2	2.623 8
4#	$y=-0.635\ 2x-2.313\ 5$	0.999 1	−0.635 2	2.364 8

发育程度相近;大孔孔容占最大(57.44%~62.47%)、微孔(15.52%~17.51%)、过渡孔孔容相对较小(16.15%~17.31%),中孔孔容最小(4.57%~9.93%);比表面积分布主要来自于微孔和过渡孔,其中微孔占主导(72.96%~74.27%),中孔和大孔的比重甚微;从分布曲线看出,随着孔径的增加比表面积逐渐减小,结果表明以上几处矿井煤层的微孔吸附能力最强。

(2)利用液氮吸附法对上述煤样进一步分析,得到中值孔径最小的 3#煤样的 BJH 总孔容、BJH 总比表面积和 BET 总比表面积也最大,其吸附能力也最强,其挥发分相对较高;中值孔径最大的 1#煤样BJH 总孔容、BJH 总比表面积和 BET 总比表面积也最小,其吸附能力也最弱,同时其挥发分最小。表明变质程度愈高,介孔发育愈广泛,孔容、比表面积愈大,吸附能力也愈强。

(3)不同埋深中阶煤孔隙结构存在一定差异,基于压汞法测定比表面积、孔容与埋深曲线呈开口朝上的凹函数变化,随埋深增大,先减小再增大;基于液氮法测定比表面积与埋深曲线呈开口朝上的凹函数变化,随埋深增大,先减小再增大;孔容随埋深增加而减小。Menger 分形维数与埋深曲线呈凸函数变化,随埋深的增加先增加后减小,而 FHH 分形维数与埋深曲线呈单调递减的变化趋势。

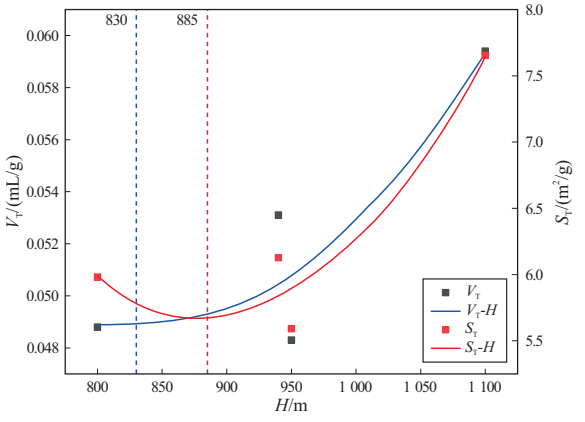

图 8 典型矿区深部主采煤层埋深与总孔容、总比表面积关系(压汞法)

Fig.8 Relationship between burial depth, pore volume, and specific surface area of deep main coal seams in typical mining areas (mercury intrusion method)

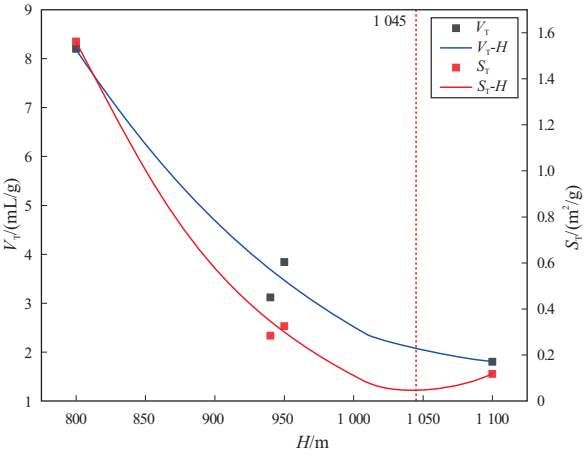

图 9 典型矿区深部主采煤层埋深与总孔容、总比表面积关系(液氮法)

Fig.9 Relationship between burial depth, pore volume, and specific surface area of deep main coal seams in typical mining areas (liquid nitrogen adsorption method)

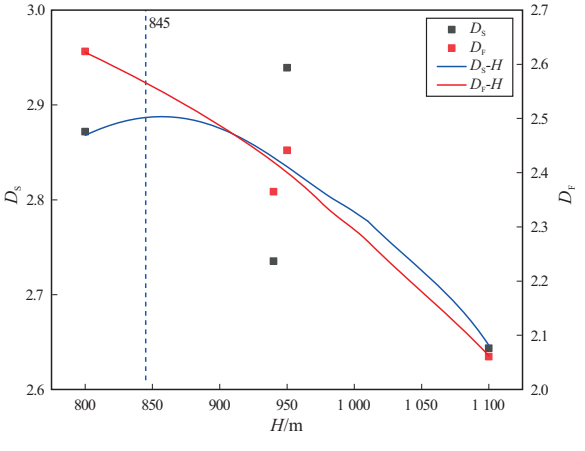

图 10 典型矿区深部主采煤层埋深与分形维数关系

Fig.10 Relationship between burial depth and fractal dimensions of deep main coal seams in typical mining areas

利益冲突声明/Conflict of Interests

所有作者声明不存在利益冲突。

All authors declare no relevant conflict of interests.

作者贡献/Authors' Contributions

李奇参与实验设计;乔磊完成实验操作;李奇与吴勇参与论文写作和修改。所有作者均阅读并同意最终稿件的提交。

The study was designed by LI Qi. The experimental operation was completed by QIAO Lei. The manuscript was drafted and revised by LI Qi and WU Yong. All authors have read the final version of the paper and consented to its submission.

参考文献:

[1] YAO Yanbin, LIU Dameng, CAI Yidong, et al. Advanced characterization of pores and fractures in coals by nuclear magnetic resonance and X-ray computed tomography[J]. Science China (Earth Sciences), 2010, 53(6): 854-862.

[2] LI Qi, WU Yong, QIAO Lei. Comprehensive characterization and metamorphic control analysis of full apertures in different coal ranks within deep coal seams[J]. Applied Sciences, 2024, 14(18): 8566.

[3] YAO Yanbin, LIU Dameng, CHE Yao, et al. Non-destructive characterization of coal samples from China using microfocus X-ray computed tomography[J]. International Journal of Coal Geology, 2009, 80(2): 113-123.

[4] LI Qi, QIN Yujin, REN Shaokui. Structural characterization analysis and macromolecular model construction of coal from Qinggangping coal mine[J]. Scientific Reports, 2023, 13(1): 14365.

[5] 秦雷,王平,翟成,等.基于氮气吸附法和压汞法低温液氮冻结煤体分形特征研究[J].采矿与安全工程学报,2023,40(1):184-193.
QIN Lei, WANG Ping, ZHAI Cheng, et al. Research on fractal characteristics of coal freezing with low temperature liquid nitrogen using nitrogen adsorption method and mercury intrusion method[J]. Journal of Mining & Safety Engineering, 2023, 40(1): 184-193.

[6] 楚亚培,张东明,王满,等.基于核磁共振技术和压汞法的液氮冻融煤体孔隙结构损伤演化规律试验研究[J].岩石力学与工程学报,2022,41(9):1820-1831.
CHU Yapei, ZHANG Dongming, WANG Man, et al. Experiment study on influence of liquid nitrogen freeze-thaw on pore structure of coal based on nuclear magnetic resonance technology and mercury intrusion methods[J]. Chinese Journal of Rock Mechanics and Engineering, 2022, 41(9): 1820-1831.

[7] 申艳军,王旭,赵春虎,等.榆神府矿区富油煤多尺度孔隙结构特征[J].煤田地质与勘探,2021,49(3):33-41.
SHEN Yanjun, WANG Xu, ZHAO Chunhu, et al. Experimental study on multi-scale pore structure characteristics of tar-rich coal in Yushenfu mining area[J]. Coal Geology & Exploration, 2021, 49(3): 33-41.

[8] 杨明,柳磊,刘佳佳,等.中阶煤孔隙结构的氮吸附—压汞—核磁共振联合表征研究[J].煤炭科学技术,2021,49(5):67-74.
YANG Ming, LIU Lei, LIU Jiajia, et al. Study on joint characterization of pore structure of middle-rank coal by nitrogen adsorption-mercury intrusion-NMR[J]. Coal Science and Technology,

2021,49(5):67-74.

[9] 聂百胜,马延崑,何学秋,等.煤与瓦斯突出微观机理探索研究[J].中国矿业大学学报,2022,51(2):207-220.
NIE Baisheng,MA Yankun,HE Xueqiu,et al.Micro-scale mechanism of coal and gas outburst:a preliminary study[J].Journal of China University of Mining & Technology,2022,51(2):207-220.

[10] 孙家广,赵贤正,桑树勋,等.基于光学显微观测的煤层裂隙发育特征、成因及其意义:以沁水盆地南部 3#煤层为例[J].断块油气田,2016,23(6):738-744.
SUN Jiaguang,ZHAO Xianzheng,SANG Shuxun,et al.Development characteristics,origins and significance of coal seam fractures under optical microscope:taking coal seam 3# in southern Qinshui Basin as an example[J].Fault-Block Oil & Gas Field,2016,23(6):738-744.

[11] 张宁远,姚素平.脆性变形序列构造煤纳米孔隙和粗糙度的原子力显微镜研究[J].煤田地质与勘探,2022,50(5):32-42.
ZHANG Ningyuan,YAO Suping.Nanopore structure and surface roughness in brittle tectonically deformed coals explored by atomic force microscopy[J].Coal Geology & Exploration,2022,50(5):32-42.

[12] PAN Jienan,WANG Kai,HOU Quanlin,et al.Micro-pores and fractures of coals analysed by field emission scanning electron microscopy and fractal theory[J].Fuel,2016,164:277-285.

[13] 赵迪斐,郭英海,毛潇潇,等.基于压汞、氮气吸附与 FE-SEM 的无烟煤微纳米孔特征[J].煤炭学报,2017,42(6):1517-1526.
ZHAO Difei,GUO Yinghai,MAO Xiaoxiao,et al.Characteristics of macro-nanopores in anthracite coal based on mercury injection,nitrogen adsorption and FE-SEM[J].Journal of China Coal Society,2017,42(6):1517-1526.

[14] 杨青,李剑,田文广,等.海拉尔盆地褐煤全孔径结构特征及影响因素[J].天然气地球科学,2020,31(11):1603-1614.
YANG Qing,LI Jian,TIAN Wenguang,et al.Characteristics on pore structures on full scale of lignite and main controlling factors in Hailar Basin[J].Natural Gas Geoscience,2020,31(11):1603-1614.

[15] 张文政,王经玺.基于显微 CT 的不同煤种微观孔隙结构综合表征[J].煤炭科学技术,2021,49(S2):85-92.
ZHANG Wenzheng,WANG Jingxi.Characterization of microscopic pore structure of different coal types based on micro CT[J].Coal Science and Technology,2021,49(S2):85-92.

[16] 杨明,柳磊,张学博,等.不同阶煤孔隙结构与流体特性的核磁共振试验研究[J].中国安全科学学报,2021,31(1):81-88.
YANG Ming,LIU Lei,ZHANG Xuebo,et al.Nuclear magnetic resonance experimental study on pore structure and fluid characteristics of coal at different ranks[J].China Safety Science Journal,2021,31(1):81-88.

[17] 翟成,孙勇,范宜仁,等.低场核磁共振技术在煤孔隙结构精准表征中的应用与展望[J].煤炭学报,2022,47(2):828-848.
ZHAI Cheng,SUN Yong,FAN Yiren,et al.Application and prospect of low-field nuclear magnetic resonance technology in accurate characterization of coal pore structure[J].Journal of China Coal Society,2022,47(2):828-848.

[18] 孙英峰,赵毅鑫,王欣,等.基于同步辐射装置定量表征煤孔隙结构非均质性和各向异性[J].石油勘探与开发,2019,46(6):1128-1137.
SUN Yingfeng,ZHAO Yixin,WANG Xin,et al.Synchrotron radiation facility-based quantitative evaluation of pore structure heterogeneity and anisotropy in coal[J].Petroleum Exploration and Development,2019,46(6):1128-1137.

[19] 蒋静宇,程远平,张硕.低阶煤孔隙结构定量表征及瓦斯吸附放散特性[J].煤炭学报,2021,46(10):3221-3233.
JIANG Jingyu,CHENG Yuanping,ZHANG Shuo.Quantitative characterization of pore structure and gas adsorption and diffusion properties of low-rank coal[J].Journal of China Coal Society,2021,46(10):3221-3233.

[20] 张驰,关平,张济华,等.分形理论表征非常规油气储层孔隙结构特征研究进展[J].北京大学学报(自然科学版),2023,59(5):897-908.
ZHANG Chi,GUAN Ping,ZHANG Jihua,et al.A review of the progress on fractal theory to characterize the pore structure of unconventional oil and gas reservoirs[J].Acta Scientiarum Naturalium Universitatis Pekinensis,2023,59(5):897-908.

[21] MANDELBROT B.How long is the coast of Britain? Statistical self-similarity and fractional dimension[J].Science,1967,156(3775):636-638.

[22] MANDELBROT B B.On the geometry of homogeneous turbulence,with stress on the fractal dimension of the iso-surfaces of scalars[J].Journal of Fluid Mechanics,1975,72(3):401-416.

[23] 陈向军,赵伞,司朝霞,等.不同变质程度煤孔隙结构分形特征对瓦斯吸附性影响[J].煤炭科学技术,2020,48(2):118-124.
CHEN Xiangjun,ZHAO San,SI Zhaoxia,et al.Fractal characteristics of pore structure of coal with different metamorphic degrees and its effect on gas adsorption characteristics[J].Coal Science and Technology,2020,48(2):118-124.

[24] 王秀娟,要惠芳,李伟,等.基于热力学模型的煤孔隙结构分形表征[J].煤田地质与勘探,2014,42(6):20-23.
WANG Xiujuan,YAO Huifang,LI Wei,et al.Fractal characterization of pore structure in coals based on thermodynamics model[J].Coal Geology & Exploration,2014,42(6):20-23.

[25] 杨师宇,姚艳斌,魏韧,等.乌鲁木齐河东矿区煤储层渗流孔孔隙分形特征研究[J].煤炭科学技术,2020,48(8):175-183.
YANG Shiyu,YAO Yanbin,WEI Ren,et al.Study on fractal characteristics of seepage pores of coal reservoirs in Hedong mining area of Urumqi[J].Coal Science and Technology,2020,48(8):175-183.

[26] 刘怀谦,王磊,谢广祥,等.煤体孔隙结构综合表征及全孔径分形特征[J].采矿与安全工程学报,2022,39(3):458-469.
LIU Huaiqian,WANG Lei,XIE Guangxiang,et al.Comprehensive characterization and full pore size fractal characteristics of coal pore structure[J].Journal of Mining & Safety Engineering,2022,39(3):458-469.

[27] KROHN C E.Fractal measurements of sandstones,shales,and carbonates[J].Journal of Geophysical Research:Solid Earth,1988,93(B4):3297-3305.

[28] 李俊键,刘洋,高亚军,等.微观孔喉结构非均质性对剩余油分布形态的影响[J].石油勘探与开发,2018,45(6):1043-1052.

LI Junjian, LIU Yang, GAO Yajun, et al. Effects of microscopic pore structure heterogeneity on the distribution and morphology of remaining oil[J]. Petroleum Exploration and Development, 2018, 45(6): 1043-1052.

[29] 贺伟,钟孚勋,贺承祖,等.储层岩石孔隙的分形结构研究和应用[J].天然气工业,2000,20(2):67-70.
HE Wei, ZHONG Fuxun, HE Chengzu, et al. Fractal texture research on the pores in reservoir rocks and its application[J]. Natural Gas Industry, 2000, 20(2): 67-70.

[30] 薛海腾,李希建,陈刘瑜,等.黔西突出煤的微观孔隙分形特征及其对渗透率的影响[J].煤炭科学技术,2021,49(3):118-122.
XUE Haiteng, LI Xijian, CHEN Liuyu, et al. Micro-pore fractal characteristics of outburst coal in western Guizhou and its influence on permeability[J]. Coal Science and Technology, 2021, 49(3): 118-122.

[31] PFEIFER P, WU Y J, COLE M W, et al. Multilayer adsorption on a fractally rough surface[J]. Physical Review Letters, 1989, 62(17): 1997-2000.

[32] 周三栋,刘大锰,蔡益栋,等.低阶煤吸附孔特征及分形表征[J].石油与天然气地质,2018,39(2):373-383.
ZHOU Sandong, LIU Dameng, CAI Yidong, et al. Characterization and fractal nature of adsorption pores in low rank coal[J]. Oil & Gas Geology, 2018, 39(2): 373-383.

[33] HU Song, SUN Xuexin, XIANG Junzheng, et al. Correlation characteristics and simulations of the fractal structure of coal char[J]. Communications in Nonlinear Science and Numerical Simulation, 2004, 9(3): 291-303.

[34] HU Song, LI Min, JUN Xiang, et al. Fractal characteristic of three Chinese coals[J]. Fuel, 2004, 83(10): 1307-1313.

[35] 熊益华,周尚文,焦鹏飞,等.基于低温 CO_2 吸附的煤和页岩微孔结构分形分析[J].天然气地球科学,2020,31(7):1028-1040.
XIONG Yihua, ZHOU Shangwen, JIAO Pengfei, et al. Fractal analysis of micropore structures in coal and shale based on low-temperature CO_2 adsorption[J]. Natural Gas Geoscience, 2020, 31(7): 1028-1040.

[36] 郝晋伟,李阳.构造煤孔隙结构多尺度分形表征及影响因素研究[J].煤炭科学技术,2020,48(8):164-174.
HAO Jinwei, LI Yang. Research on multi-scale fractal characteristics of pore structure in tectonic coal and analysis of its influence factors[J]. Coal Science and Technology, 2020, 48(8): 164-174.

[37] 于不凡.煤矿瓦斯灾害防治及利用技术手册[M].北京:煤炭工业出版社,2005.
YU Bufan. Technical manual for prevention and utilization of coal mine gas disasters[M]. Beijing: China Coal Industry Publishing House, 2005.

[38] YU Song, JIANG Bo, PEI Shao, et al. Matrix compression and multifractal characterization for tectonically deformed coals by Hg porosimetry[J]. Fuel, 2018, 211: 661-675.

[39] WASHBURN E W. The dynamics of capillary flow[J]. Physical Review, 1921, 17(3): 273-283.

[40] LEON C A L. New perspectives in mercury porosimetry[J]. Advances in Colloid and Interface Science, 1998, 76: 341-372.

[41] FALLICO C, TARQUIS A M, DE BARTOLO S, et al. Scaling analysis of water retention curves for unsaturated sandy loam soils by using fractal geometry[J]. European Journal of Soil Science, 2010, 61(3): 425-436.

[42] HODOT B B. Outburst of coal and coalbed gas[M]. Beijing: China Industry Press, 1966: 310-318.

[43] OUQUEROL J, AVNIR D, FAIRBRIDGE C W, et al. Recommendations for the characterization of porous solids (Technical report)[J]. Pure and Applied Chemistry, 1994, 66(8): 1739-1758.

[44] PFEIFER P, AVNIR D. Chemistry in noninteger dimensions between two and three. I. Fractal theory of heterogeneous surfaces[J]. The Journal of Chemical Physics, 1983, 79(7): 3558-3565.

[45] AVNIR D, JARONIEC M. An isotherm equation for adsorption on fractal surfaces of heterogeneous porous materials[J]. Langmuir, 1989, 5(6): 1431-1433.

[46] JARONIEC M. Evaluation of the fractal dimension from a single adsorption isotherm[J]. Langmuir, 1995, 11(6): 2316-2317.

[47] 谢和平.分形—岩石力学导论[M].北京:科学出版社,1996.
XIE Heping. Introduction to fractal rock mechanics[M] Beijing: Science Press, 1996.

[48] 陈静,崔啸,王磊,等.不同埋深煤体孔隙结构特征及瓦斯吸附特性研究[J].矿业研究与开发,2023,43(3):166-171.
CHEN Jing, CUI Xiao, WANG Lei, et al. Study on pore structure characteristics and gas adsorption characteristics of coal body with different buried depths[J]. Mining Research and Development, 2023, 43(3): 166-171.

[49] 冯翠荣,马海军,李彦朋.呼和湖凹陷煤层气地质条件及资源潜力分析[J].科学技术与工程,2018,18(26):17-24.
FENG Cuirong, MA Haijun, LI Yanpeng. Geological conditions and resource potential analysis of coalbed methane in the Huhehu Depression[J]. Science Technology and Engineering, 2018, 18(26): 17-24.

[50] 陆小霞,黄文辉,陈燕萍,等.沁水盆地南部深煤层孔隙结构特征[J].东北石油大学学报,2015,39(3):41-49.
LU Xiaoxia, HUANG Wenhui, CHEN Yanping, et al. Pore structure of deep coal seam in southern Qinshui Basin[J]. Journal of Northeast Petroleum University, 2015, 39(3): 41-49.

[51] 刘长江,张琨,宋璠.CO_2 地质埋藏深度对高阶煤孔隙结构的影响[J].煤田地质与勘探,2018,46(5):32-36.
LIU Changjiang, ZHANG Kun, SONG Fan. Influences of burial depth on pore structure of high-rank coal during the CO_2 storage process[J]. Coal Geology & Exploration, 2018, 46(5): 32-36.

[52] 申建.论深部煤层气成藏效应[J].煤炭学报,2011,36(9):1599-1600.
SHEN Jian. CBM-reservoiring effect in deep strata[J]. Journal of China Coal Society, 2011, 36(9): 1599-1600.

[53] 孟召平,田永东,李国富.沁水盆地南部煤储层渗透性与地应力之间关系和控制机理[J].自然科学进展,2009,19(10):1142-1148.
MENG Zhaoping, TIAN Yongdong, LI Guofu. The relationship and control mechanism between permeability and geostress of coal reservoirs in the southern Qinshui Basin[J]. Progress in Natural Sciences, 2009, 19(10): 1142-1148.

(编辑 张玲珑)